Catalysis Science & Technology

ROYAL SOCIETY OF CHEMISTRY

PAPER

View Article Online
View Journal | View Issue

Cite this: *Catal. Sci. Technol.*, 2023, 13, 2349

Supported silver and copper catalysts in the oxidative dehydrogenation of methanol to formaldehyde: a comparative study under industrially relevant conditions†

Fabian Eichner,[a] Emre Turan,[a] Jörg Sauer,[a] Michael Bender[b] and Silke Behrens *[a]

In this study, we compare and assess the performance of silver and copper species in methanol oxidative dehydrogenation (ODH) to formaldehyde. Methanol ODH over polycrystalline silver catalysts is a major industrial synthesis route for formaldehyde today. Ag/SiO_2, Ag/TiO_2, Ag/ZrO_2, Cu/SiO_2, Cu/TiO_2 and Cu/ZrO_2 catalysts were prepared by strong electrostatic adsorption (SEA) and employed in the methanol ODH. All catalysts showed metal species homogenously distributed over the metal support and metal weight fractions up to 3.86% Ag and 7.96% Cu after sequential SEA steps. The silica-supported catalysts revealed the best performance in methanol ODH with the highest formaldehyde selectivities and stable conversions after seven hours time-on-stream. For these catalysts, the performance of silver and copper species in methanol ODH was further studied and compared close to industrial operating conditions. At low methanol feed concentrations, the Ag/SiO_2 catalyst revealed a superior performance while at higher methanol feed fractions, the Cu/SiO_2 catalyst showed improved performance and higher formaldehyde yields.

Received 8th August 2022,
Accepted 12th March 2023

DOI: 10.1039/d2cy01405j

rsc.li/catalysis

Introduction

Production capacities exceeding 30 million tons per year indicate the outstanding importance of formaldehyde in today's chemical industry.[1] Formaldehyde is used as a platform chemical for the production of resins,[2] plastics[3] and various other chemicals.[4–7] A large part of formaldehyde today is manufactured *via* oxidative dehydrogenation of methanol over polycrystalline silver catalysts.[8,9] The so-called silver process combines highly selective formaldehyde formation, simple catalyst regeneration and smaller equipment costs compared to other formaldehyde synthesis routes.[8] Typically, the process is carried out by passing a mixture of gaseous methanol, steam and air over a catalyst bed at ambient pressure and temperatures in the range of 560 to 700 °C.[8,10] The catalyst bed consists of polycrystalline silver particles with different grain sizes ordered in horizontal layers in a cylindrical bed with several meters diameter.[8,11] The total height of the bed ranges from 20 to 30 mm. Typically, methanol is introduced in excess with molar methanol-oxygen ratios between 2.3 and 4 depending on the process configuration.[8] To minimize thermal decomposition of formaldehyde, the product mixture is rapidly quenched after reaction and very short residences times are established with gas-hourly space velocities up to 250 000 h^{-1}. Formaldehyde yields at industrial conditions range from 82 to 92%.[8,10,11] After absorption in water, the product is present in aqueous solution with typical weight percentages between 37 and 55%.[2]

The main reactions in methanol ODH are described in Scheme 1.[12–17] While successfully applied in industry for several decades, the mechanism is still not fully understood.[12–16,18,19] Especially the question if methanol conversion proceeds *via* direct dehydrogenation (reaction (1)), partial oxidation (reaction (2)) or a combination of both mechanisms remains unanswered. There is broad agreement on the pre-treatment and structure sensitivity of the catalytic

(1) $CH_3OH_{(g)}$	⇌	$H_2CO_{(g)} + H_{2(g)}$	$\Delta H^0 = +84\ kJmol^{-1}$
(2) $CH_3OH_{(g)} + 0.5\ O_2$	→	$H_2CO_{(g)} + H_2O_{(g)}$	$\Delta H^0 = -159\ kJmol^{-1}$
(3) $H_2CO_{(g)} + O_2$	→	$CO_{2(g)} + H_2O_{(g)}$	$\Delta H^0 = -514\ kJmol^{-1}$
(4) $H_{2(g)} + 0.5\ O_2$	→	$H_2O_{(g)}$	$\Delta H^0 = -243\ kJmol^{-1}$
(5) $H_2CO_{(g)}$	⇌	$CO_{(g)} + H_{2(g)}$	$\Delta H^0 = +12\ kJmol^{-1}$

Scheme 1 Reactions relevant in the methanol ODH on silver catalysts.

[a] *Institute of Catalysis Research and Technology, Karlsruhe Institute of Technology (KIT), Hermann-von-Helmholtz-Platz 1, D-76344 Eggenstein-Leopoldshafen, Germany. E-mail: silke.behrens@kit.edu*
[b] *BASF SE, Carl-Bosch-Straße 38, D-67056 Ludwigshafen am Rhein, Germany*

† Electronic supplementary information (ESI) available. See DOI: https://doi.org/10.1039/d2cy01405j

reaction,[17,19–24] reaction induced changes in catalyst morphology[17,20,22–28] and the presence of different surface and sub-surface oxygen species with distinct electronic states.[13,14,20,25,27–36] However, their role during reaction and their influence on the nature of the actual active sites is not fully clarified. Wachs and Madix used temperature programmed reaction spectroscopy to study methanol ODH on Ag(110) single crystals.[12] They showed that dissociative adsorption of methanol on blank silver is negligible, but adsorption is enhanced upon presence of adsorbed oxygen. Although adsorbed oxygen is not needed for reaction (1) from a stoichiometric point of view, it is necessary to enable methanol adsorption in the first place. Furthermore, methoxy species are identified as important intermediates. Their formation goes along with hydrogen atom abstraction from the hydroxyl group and is followed by water formation. The decomposition of methoxy species leads to the formation of formaldehyde and hydrogen species, its reaction with oxygen to the formation of formaldehyde and water species. Excess oxygen tends to oxidize formaldehyde on the silver surface leading to carbon dioxide and water (reaction (3)). The complete oxidation of methanol is not observed. The findings of Wachs and Madix are supported by various experimental and theoretical studies.[13,15,28] The formation of carbon monoxide (reaction (5)) taking place as a homogeneous gas-phase reaction is not a catalytic process and depends on overall residence time, gas-phase temperature and the presence of local hotspots.[13,16,17] The oxidation of hydrogen as displayed in reaction (4) is reported by different groups.[16,17,19] For example, Nagy and coworkers identified hydrogen oxidation in the subsurface region followed by water diffusion to the surface and desorption.[23,27]

Polycrystalline copper exhibits similar catalytic activity in methanol ODH to formaldehyde with selectivities in the range of 80 to 90%.[37] Previous to polycrystalline silver, copper catalysts were used frequently in the industrial process. They reveal a product spectrum and reaction mechanism comparable to silver catalysts.[38,39] Similar to the silver–oxygen system, the existence of surface and sub-surface oxygen species was emphasized for copper under methanol dehydrogenation conditions.[40] A study of Thomas performed in the 1920s is the sole work available to assess the relative activity of silver and copper in methanol ODH.[41] There, methanol dehydrogenation was investigated over silver and copper spirals without direct measurement of the reaction temperature. Based on the yields (74% for silver and 65% for copper) Thomas concluded that silver was more active than copper. However, the maximum yields were identified for molar methanol-oxygen ratios (1 to 1.25 for silver, 0.76 to 0.9 for copper) which is way out of the industrially applied range of 2.3 to 4. To the best of our knowledge, the behavior of silver and copper catalysts in methanol ODH to formaldehyde has never been compared under reaction conditions close to those of the industrial process.

The comparison of the bulk metal catalysts is difficult, and usually, supported catalysts are more suitable for this purpose. Both incipient wetness impregnation (IWI) and ion exchange (IE) methods are reported for the preparation of supported silver catalysts, *e.g.* on SiO_2, Al_2O_3, TiO_2, CeO_2, MgO, ZrO_2, Nb_2O_5 and activated carbon.[42–44] Chemical reduction is reported for the preparation of Ag/SiO_2,[45,46] $Ag/TiO_2–SiO_2$,[47] $Ag/SiO_2–Al_2O_3$ [48,49] and Ag/SBA-15 catalysts.[50] As previously emphasized by Regalbuto and coworkers, traditional procedures for preparation of supported silver catalysts like wet impregnation of silver salts in combination with high temperature treatments offer only limited control over particle size.[44] Recently, supported silver catalysts in methanol ODH have been optimized by developing titania-supported silver nanoparticles (NPs),[51] silver deposited on titania nanofibers and doped with Congo-red NPs,[52] silver metal fibers and composite Ag/carbon fibers synthesized by electrospinning,[53] mesostructured cellular foams to fixate bimetallic AuAg catalysts[54] and bimetallic Ag-in-Au NPs embedded in porous silica.[55] Similar to silver catalysts, supported copper catalysts were prepared previously both by IWI and IE methods.[56–61] Recently, Florek-Milewska *et al.* have modified mesoporous sieves of SBA-3 type with copper species by a wet impregnation method.[62]

Despite the recent advances in the synthesis of new catalyst configurations for both silver and copper systems, a preparation method suitable to compare both metals in methanol ODH should be simple and meet the requirements of the specific reaction conditions. As already pointed out, residence times in the industrial application are kept as low as possible due to the reactivity of formaldehyde both in reaction with excess oxygen and thermal decomposition. Therefore, active species with homogeneous dispersion and particle sizes in the lower nanometer range as well as strong metal–support interactions limiting the mobility of active species at the high temperatures of the catalyst pretreatment and the reaction itself are favorable.

Strong electrostatic adsorption (SEA) was recently shown to achieve homogeneous metal dispersions with a relatively simple preparation procedure for silver NPs on SiO_2, Al_2O_3, ZrO_2, Nb_2O_5 and activated carbon.[44] SEA was also applied to produce Cu/SiO_2 catalysts and compared to IWI.[63] Average particle sizes achieved were considerably lower for SEA (2.4 nm average) than for IWI (4.5 nm average). The principles explaining the characteristics of SEA were described previously in great detail.[64] For all oxides in aqueous solution a point of zero charge exists (PZC), where the protonation-deprotonation of hydroxyl groups of the support surface is in equilibrium and thus the overall surface charge is zero. If the pH value of the solution is below the pH value at the point of zero-charge (pH_{PZC}), the majority of hydroxyl groups are protonated and the electrostatic adsorption of anionic complexes is possible. If the pH value is above the pH_{PZC}, the majority of hydroxyl groups are deprotonated and the electrostatic adsorption of positive metal complexes can be performed. Coinage-metal catalysts such as Cu/SiO_2, Ag/SiO_2 and Ag/ZrO_2 were prepared by SEA *via* adsorption of diammine silver(I) ($(Ag(NH_3)_2)^+$) and tetraammine copper(II) ($(Cu(NH_3)_4)^{2+}$) complexes.[44,63]

Within the present study, we address the preparation of supported Ag and Cu catalysts with good stability by SEA. The performance of the catalysts is evaluated for different support materials (*i.e.* SiO_2, TiO_2, ZrO_2) and metal loadings in methanol ODH to formaldehyde and studied under conditions close to the industrial conditions (*i.e.* methanol feed fractions up to 13.1 mol%). The catalysts are characterized by several analytical tools including transmission electron microscopy (STEM-HAADF), powder X-ray diffraction, and N_2 physisorption.

Experimental section

Details on all used materials are provided in the ESI† (S1.1).

Catalyst synthesis *via* SEA

The pH_{PZC} of each support was determined by adapting a procedure presented by Park and Regalbuto and is described in detail in the ESI† (S1.2).[64] Adsorption of active species *via* SEA was performed by adding a metal precursor solution to the support material. Details for the preparation of the silver diammine (AgDA) and the copper tetraammine (CuTA) solution (200 ppm) are provided in the ESI† (S1.2). Concentrations of support surface area (CSA) in the range of 500 to 4000 $m^2\ L^{-1}$ were used and calculated as follows:

$$\mathrm{CSA} = A_{\mathrm{BET}} \cdot \frac{m_{\mathrm{support}}}{V_{\mathrm{solution}}}$$

where, A_{BET} [$m^2\ g^{-1}$] is the specific surface area of the support material, m_{support} [g] the mass of support material and V_{solution} [L] the volume of precursor solution. The solution was then shaken for one hour at 170 rpm on an orbital shaker. Afterwards, the catalyst was isolated and the supernatant collected by centrifugation (10 000 rcf, 15 min) and the catalyst was dried at 100 °C overnight. The metal uptake by the support material was determined by measuring the metal concentration in the solution before and after SEA with inductively coupled plasma-optical emission spectroscopy (ICP-OES) (ICP-OES 700 series, Agilent Technologies). The adsorption density (Γ_{metal}) and the weight fraction of metal (w_{metal}) adsorbed onto the support was determined as follows:

$$\Gamma_{\mathrm{metal}} = \frac{\left(\beta_{\mathrm{metal,initial}} - \beta_{\mathrm{metal,final}}\right)}{M_{\mathrm{metal}} \cdot \mathrm{CSA}}$$

$$w_{\mathrm{metal}} = \left(\beta_{\mathrm{metal,initial}} - \beta_{\mathrm{metal,final}}\right) \cdot \frac{V_{\mathrm{solution}}}{m_{\mathrm{catalyst,total}}}$$

here, $\beta_{\mathrm{metal,initial}}$ and $\beta_{\mathrm{metal,final}}$ [$g\ L^{-1}$] are the initial and final concentrations of metal in solution. M_{metal} [$g\ mol^{-1}$] is the molar mass of the metal, V_{solution} [L] the volume of precursor solution and $m_{\mathrm{catalyst,total}}$ [g] the total weight of the catalyst sample. The dried catalyst was compacted with a hydraulic press using a pressing force of 5 t m^{-2} and sieved to a grain-size fraction of 224–400 μm.

Characterization

To determine the specific surface area of the supports, nitrogen physisorption was performed at 77 K using a Quantachrome NovaWin. The samples were degassed at 230 °C for 20 h before measurement. The surface area was quantified using the model of Brunauer–Emmett–Teller (BET). To address the nature of the metal complexes in the precursor solutions, UV-vis spectroscopy was applied using a Specord S600 (AnalytikJena). For qualitative determination of the silver and copper complexes, a concentrated AgDA solution (1500 ppm) and a CuTA solution (200 ppm) was used, respectively.

Powder X-ray diffraction (XRD) measurements were performed with an X'Pert PRO PANalytical (Malvern Panalytical) using Cu Kα radiation (λ = 0.15418 nm). All samples were scanned for 40 min between 10° and 80° (2θ). Particle sizes were estimated with the Scherrer equation using a shape factor of 0.9. Scanning electron microscopy (SEM) was performed using a Zeiss GeminiSEM 500 equipped with a Schottky field emission cathode. For imaging, secondary electron detectors (Everhardt-Thornley, Inlens) and back-scattering electron detectors were used. For energy-dispersive X-ray spectroscopy (EDX), an Oxford X-Max System with 80 m^2 of active crystal area was used. Transmission electron spectroscopy (TEM) and scanning transmission electron microscopy (STEM) were performed at the FEI Tecnai Osiris ChemieSTEMTM electron microscope (Laboratory for Electron Microscopy, KIT), equipped with a high-angle annular dark field (HAADF) detector (200 kV). Samples were prepared by grinding the catalyst und suspending it in distilled water. One drop of the suspension was put onto a carbon-coated gold grid and dried. Element distributions were determined by EDX.

Catalytic testing

The catalytic tests were carried out in an electrically heated, continuous flow reactor with a heated length of 30 cm at temperatures between 500 °C and 650 °C and at ambient pressure. The reactor tube was made from quartz glass with an inner diameter of one centimeter. In all experiments the catalyst bed height was kept constant at 0.1 cm corresponding to an amount of 0.035 g for TiO_2, 0.028 g for SiO_2 and 0.1 g for ZrO_2 supported catalysts. The differences in amount resulted from the different densities of the support materials. Keeping the catalyst bed height constant is critical to ensure comparable reaction conditions in catalytic testing of methanol ODH. At the entrance on top of the catalyst bed, the reactor was filled with quartz glass spheres for improved heat transport properties. The temperature at the catalyst bed was measured with a type K thermocouple inside a closed quartz glass tube. Prior to catalytic testing, the catalysts were calcined in the flow reactor. First, the catalysts were heated in synthetic air (0.5 $L_{STP}\ min^{-1}$, 15 °C min^{-1}) up to 575 °C. Then, the temperature was kept constant for 15 minutes. Similar procedures have

been previously reported for other catalysts on methanol ODH.[16,17] The reaction temperature was approached with a heating ramp of 15 °C min^{-1} under a flow of 0.5 L_{STP} min^{-1} nitrogen. To study the influence of the reaction temperature on conversion and selectivity, the temperature was stepwise increased every hour by 25 °C until a temperature of 600–650 °C was reached. Prior to these experiments, all samples were kept for 8 hours at 500 °C to achieve steady-state activity under constant reaction conditions (*i.e.*, 2.5% methanol, 1.0% oxygen, 1 L_{STP} min^{-1} total flow rate). Synthetic air and nitrogen were dosed using thermal mass flow controllers and mixed with methanol dosed *via* a coriolis mass flow controller and evaporated in a direct evaporation device (all Bronkhorst). The gas-phase was analyzed using a two-module gas chromatograph (MicroGC Fusion, Inficon) with helium and argon as permanent gases and equipped with thermal conductivity detectors. GC measurements were repeated four times and the average values were used for evaluation. Experiments were evaluated by calculating the reactant conversions and product selectivities as follows:

$$X_i = \frac{\dot{N}_{i,0} - \dot{N}_i}{\dot{N}_{i,0}}$$

$$S_j = \frac{\dot{N}_j - \dot{N}_{j,0}}{\dot{N}_{MeOH,0} - \dot{N}_{MeOH}} \cdot \frac{\nu_{MeOH}}{\nu_j}$$

where X and S are the conversion and selectivity, respectively. $\dot{N}_0$ [mol s^{-1}] is the molar flow rate of the component entering the reactor, $\dot{N}$ [mol s^{-1}] the molar flow rate after reaction and ν the corresponding stoichiometric coefficient. Product selectivities were calculated as a function of the amount of methanol consumed.

Results and discussion

The support material needs to be stable at the high reaction temperatures and its activity in the reaction should be limited. Based on these considerations, silica, titania and zirconia were chosen as support materials in this study. The specific surface areas of the support materials determined by nitrogen physisorption were 194 m^2 g^{-1} for SiO_2, 47 m^2 g^{-1} for TiO_2 and 5 m^2 g^{-1} in case of ZrO_2, which was in good agreement with those reported previously.[44,65–67] The SEM images of the supports (Fig. 1A1 to A3) indicated an increasing size of the primary support particles from SiO_2 over TiO_2 to ZrO_2 which was consistent with the decreasing specific surface area. The pH values at the PZC measured by pH shift experiments (Fig. 1B1 to B3) were 5.9 for silica, 3.7 for titania and 4.6 for zirconia and thus, within the acidic regime and suitable for adsorption of positively charged metal complexes *via* SEA under moderate conditions (for further information see ESI† (S2.1)).

Synthesis of supported coinage-metal catalysts

The amount of metal precursor adsorbed during SEA depends on the CSA, the precursor complex species at the pH

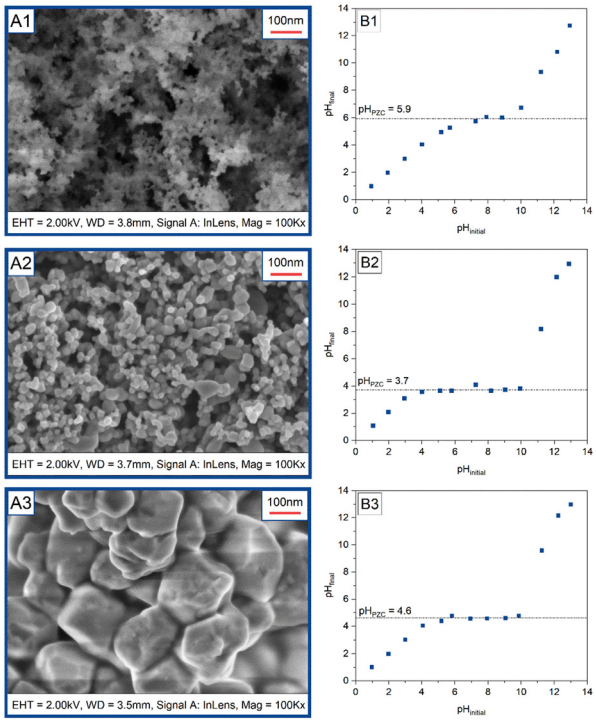

Fig. 1 SEM images of support materials (A1: SiO_2, A2: TiO_2, A3: ZrO_2) and final pH value as function of initial pH value (B1: SiO_2, B2: TiO_2, B3: ZrO_2) in PZC determination.

value of adsorption (pH_{ads}) and the difference between pH_{PZC} and pH_{ads}. In all cases, the pH value of the solution during adsorption was kept at approximately 11.5 to 11.6. Maxima in metal uptake for the silver diammine complex have been previously shown at a pH value of 10 on silica and 11.5 on zirconia.[44] On silica, the maximum uptake for the copper tetra ammine complex was at a pH value of 11.5.[63] To identify the metal complexes present in the precursor solution at the respective pH value, UV-vis spectroscopy measurements were performed. For the UV-vis spectra (ESI† S2.2, Fig. S1) of the AgDA solution, a band at 300 nm could be assigned to the aqua complex ($(Ag(H_2O)_2)^+$).[44] An absorption band was expected at 400 nm for the $(Ag(NH_3)_2)^+$ complex, but could not be detected here. Kyriakidou and coworkers recorded the molar fractions of both the aqua and diammine complexes over a wide pH range.[44] Their results indicated that at pH values above 9.5 the diammine complex was dominant and the fraction of aqua complex was negligible for pH values above 11. The UV-vis spectrum of the CuTA solution at pH 11.5 clearly showed a peak at 600 nm which could be attributed to the $(Cu(NH_3)_4)^{2+}$ complex.[68]

Catalysts with different CSA, adsorption density and metal weight fraction (Table 1) were prepared by SEA. For silver catalysts with a CSA of 1000 m^2 L^{-1}, the adsorption density was highest on titania and decreased to about a half for zirconia and silica. This was consistent with the decrease in pH_{PZC} from silica (pH_{PZC} = 5.9), zirconia (pH_{PZC} = 4.6) to titania (pH_{PZC} = 3.7) and the increasing difference between pH_{ads} and pH_{PZC}, which is known to influence the adsorption

Table 1 Summary of catalyst materials prepared in this study together with CSA, adsorption densities and weight fractions of metals

Catalyst	SEA sequences	CSA/m^2 L^{-1}	Γ_{Metal}/μmol m^{-2}	w_{metal}/%
Ag/SiO_2	1	4000	0.28	0.58
	1	2000	0.56	1.15
	1	1000	0.74	1.53
	1	500	0.93	1.90
	2	500	1.67	3.43
	3	500	1.87	3.86
Ag/TiO_2	1	4000	0.45	0.23
	1	2000	0.86	0.43
	1	1000	1.69	0.85
	1	500	2.97	1.49
	2	500	4.91	2.47
Ag/ZrO_2	1	1000	0.83	0.04
Cu/SiO_2	1	4000	0.66	0.80
	1	2000	1.39	1.69
	1	1000	1.92	2.32
	1	500	2.68	3.19
	2	500	5.26	6.27
	3	500	6.64	7.96
Cu/TiO_2	1	1000	2.89	0.86
Cu/ZrO_2	1	1000	2.84	0.09

density. Comparing the adsorption of silver and copper species at a CSA of 1000 m^2 L^{-1} showed that more copper was adsorbed than silver. One reason for this behavior could be the stronger ion potential of the $(Cu(NH_3)_4)^{2+}$ complex compared to $(Ag(NH_3)_2)^+$.[69,70] The CSA influenced the amount of adsorbed metal. Reducing the CSA from 4000 m^2 L^{-1} to 2000 m^2 L^{-1} approximately doubled the adsorption density for Ag/TiO_2, Ag/SiO_2 and Cu/SiO_2. In general, reducing the CSA increased the metal uptake. This increase was initially linear but with decreasing tendency for lower CSA. To further increase the metal loading, the procedure was repeated up to three times in a sequential SEA with the catalyst dried after each SEA cycle. After two cycles of sequential SEA, the adsorption density nearly doubled for Ag/TiO_2, Ag/SiO_2 and Cu/SiO_2, while this increase was much less after the third cycle, most probably due to surface saturation effects.

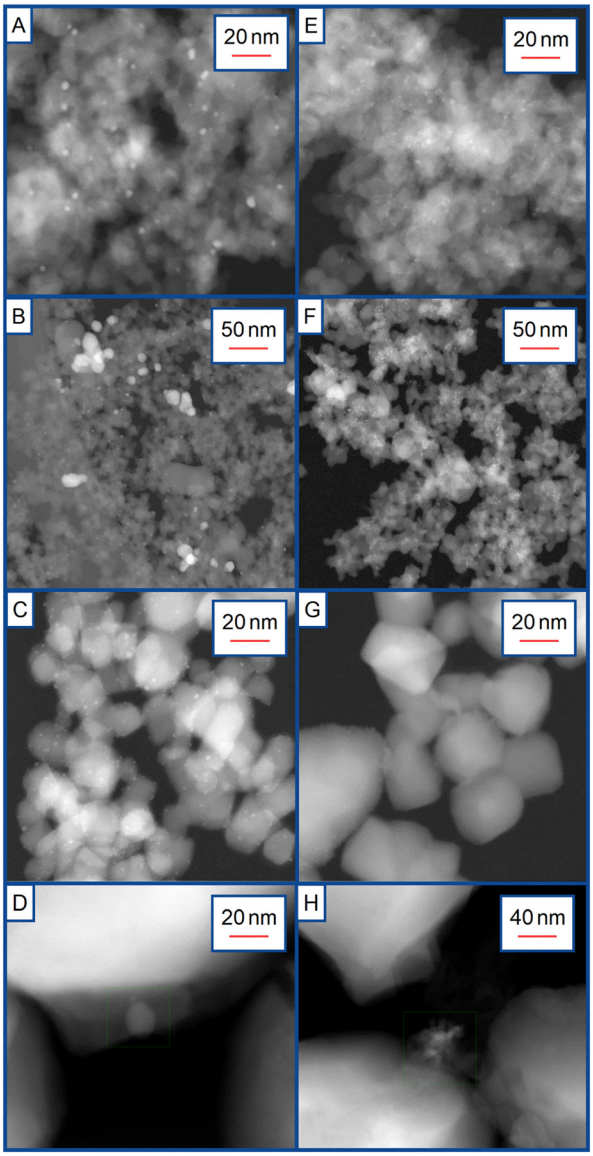

Fig. 2 STEM-HAADF images of the catalysts (A: Ag/SiO_2 1000 m^2 L^{-1}, B: Ag/SiO_2 2 × 500 m^2 L^{-1}, C: Ag/TiO_2 1000 m^2 L^{-1}, D: Ag/ZrO_2 1000 m^2 L^{-1}, E: Cu/SiO_2 1000 m^2 L^{-1}, F: Cu/SiO_2 2 × 500 m^2 L^{-1}, G: Cu/TiO_2 1000 m^2 L^{-1}, H: Cu/ZrO_2 1000 m^2 L^{-1}).

Catalyst characterization

Representative scanning transmission electron microscopy high angle annular dark field (STEM-HAADF) images of the as-prepared catalysts are presented in Fig. 2A–H (for additional STEM-HAADF images, particle size distributions and elemental maps see S2.3, Fig. S2–S4 in the ESI†). With exception of silver and copper catalysts on zirconia, the adsorbed metal complexes were readily apparent. TEM images of the Ag/SiO_2 catalyst (Fig. 2A) showed adsorbates with an average size of 8.1 nm and homogeneously dispersed over the support material, which was in good agreement with previous reports on Ag/SiO_2 catalysts.[44] For the Ag/SiO_2 catalyst prepared by sequential SEA (Fig. 2B), the average diameter was 9 nm, but the fraction of larger aggregates in the range of 10 to 50 nm is readily apparent (Fig. 2B). Ag/TiO_2 (Fig. 2C) consisted of homogeneously dispersed adsorbates with smaller sizes (1–3 nm). Cu/SiO_2 (Fig. 2E) indicated very small, well dispersed adsorbates (1.6 nm in average), and no increase in adsorbate size was observed even after sequential steps of SEA (2 nm in average) (Fig. 2F). The adsorbates of the Cu/TiO_2 catalyst were smaller and only 1.5 nm in size (Fig. 2G). In case of Ag/ZrO_2 (Fig. 2D) and Cu/ZrO_2 (Fig. 2H), hardly any adsorbates were detected by STEM-HAADF imaging as a consequence of the very small aggregate size, the high contrast of the ZrO_2 support and/or the very low metal loading (Table 1). Elemental maps obtained from STEM-EDX spectrum imaging of Cu/ZrO_2 (see ESI,† S2.3, Fig. S2B), revealed homogeneously dispersed Cu species with sizes well below 2 nm. In general, the adsorption of the copper complex seemed to result in smaller adsorbates and more homogeneous distribution than the silver species.

Catalytic testing in oxidative dehydrogenation of methanol

Prior to the detailed catalytic testing, the systems were checked for mass transfer limitations according to an established, experimental procedure.[71] The results indicated that neither internal nor external mass transfer limitations influenced the catalytic testing under the applied conditions.

To determine the principle reaction behavior, temperature variation experiments were performed for all catalyst systems with a CSA of 1000 m^2 L^{-1}. Representative plots of educt conversion and product selectivity as function of reaction temperature are shown in Fig. 3. The product spectrum for Ag/SiO_2 was in good agreement with the one observed for the polycrystalline silver catalyst.[12,13,16,27] The measured products were formaldehyde (FA), carbon monoxide (CO), carbon dioxide (CO_2), hydrogen (H_2) and water (H_2O). Methanol conversion increased slightly with temperature and oxygen conversion was complete above 600 °C. Up to a temperature of 575 °C, the FA selectivity was close to 90%. The selectivity to CO_2 was below 10% and decreased with temperature. At higher temperatures, the thermal decomposition of FA became more pronounced and more CO was produced leading to a decrease in FA selectivity. As indicated previously, CO formation proceeds *via* a gas-phase reaction which is strongly dependent on temperature and residence time of the gas-phase. The more pronounced CO formation

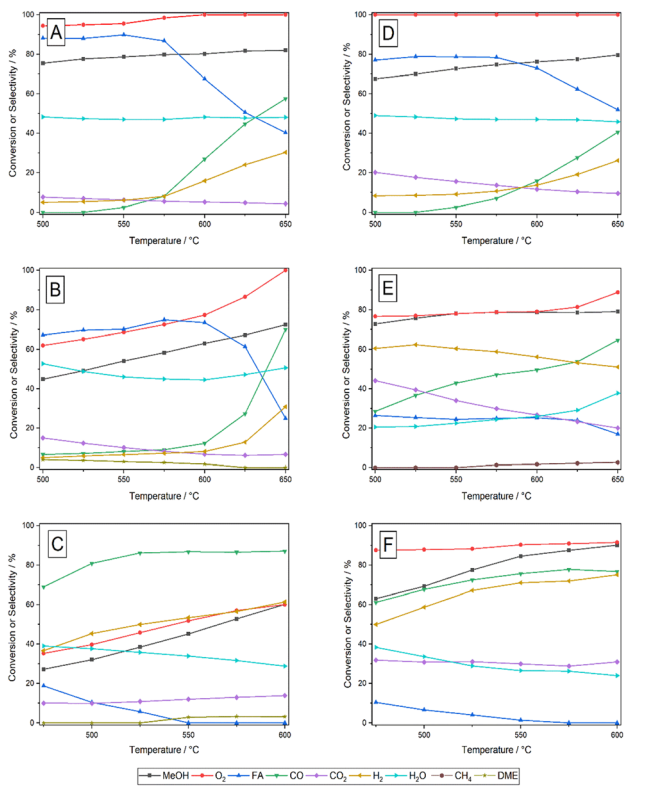

Fig. 3 Conversion and selectivity as function of temperature for Ag/SiO_2 (A), Ag/TiO_2 (B), Ag/ZrO_2 (C), Cu/SiO_2 (D), Cu/TiO_2 (E) and Cu/ZrO_2 (F) with CSA = 1000 m^2 L^{-1} in all cases. Feed: 2.5% methanol and 1.0% oxygen in nitrogen, total flow rate: 1 L_{STP} min^{-1}, TOS: 8 h.

was predominantly due to imperfect cooling and simplified catalyst bed design compared to the optimized industrial process. However, this did not affect the evaluation of the catalyst system used in this study. The Ag/TiO_2 catalyst showed a similar product spectrum except for traces of dimethyl ether (DME), which disappeared at higher temperatures. Methanol and oxygen conversion increased steadily with temperature but were considerably lower compared to the Ag/SiO_2 catalyst. It should be noted that the molar Ag content of the catalyst bed was also slightly lower in case of Ag/TiO_2. The oxygen conversion showed a non-linear increase above 600 °C which could be related to the reaction of excess oxygen with hydrogen. This was also confirmed by the increase of H_2O selectivity above 600 °C. The FA selectivity was increasing with temperature to a maximum value of 75% around 575 °C but decreased above 600 °C again due to the thermal decomposition of FA. Compared to Ag/SiO_2, the selectivity to CO_2 was considerably higher throughout the investigated temperatures and the TiO_2 support material itself exhibited a distinct activity towards FA. The Ag/ZrO_2 catalyst revealed a similar product spectrum compared to the other silver catalysts but a quite different temperature dependent behavior. The FA selectivity was very low and no FA was produced at all above 550 °C. The main product was CO with H_2 being more prominent than H_2O. This behavior was attributed to the activity of ZrO_2 itself, which catalyzed the direct oxidation of methanol to CO and H_2, in agreement with previous studies. For example, Bronkema and Bell identified CO and H_2 as major products above 327 °C studying methanol oxidation over ZrO_2 with temperature-programmed desorption.[72] Other products were CO_2 and H_2O but in smaller quantities. The catalytic activity of the pure titania and zirconia support materials is shown in Fig. S7 in the ESI† (S3.2).

For the silica-supported copper catalyst, FA, CO, CO_2, H_2 and H_2O were determined as reaction products highlighting the similar reaction mechanism to silver as proposed in previous work.[12,38,39] The FA selectivity was close to 80% up to temperatures of 575 °C. At higher temperatures thermal decomposition intensified leading to increased CO formation. Interestingly, CO formation by thermal decomposition was less pronounced on Cu/SiO_2 compared to Ag/SiO_2. The selectivity towards CO_2 started with approximately 20% at the lowest temperature and decreased to around 10% at 650 °C. This catalyst revealed a performance comparable to the industrially applied copper catalyst. In industrial application, a product ratio of FA to CO_2 around 4 : 1 was reported with FA selectivities ranging between 80 and 90%.[12,37,39] In experimental and theoretical studies, stronger bonding strength of reaction intermediates were attributed to the copper surface compared to the silver surface for identical reaction conditions.[12,73,74] This would lead to longer surface residence times on copper and thus increased the extent of consecutive CO_2 formation. The oxygen conversion was complete over the entire temperature range. The methanol conversion increased slightly with

temperature but was generally lower than for the Ag/SiO_2 catalyst although the overall Cu loading in the reactor was higher. The selectivity to H_2 was slightly higher on the Cu/SiO_2 catalyst. The Cu/TiO_2 catalyst showed pronounced differences compared to the Ag/TiO_2 and Cu/SiO_2 systems. CO_2 and CO formation was favored over FA formation with CO_2 selectivity decreasing and CO selectivity increasing with temperature. The H_2 selectivity was between 50 and 60% indicating a different catalytic behavior compared to Ag/TiO_2 and Cu/SiO_2. An additional catalytic path similar to the activity of zirconia towards CO formation could be present. Since the product spectra determined for Ag/TiO_2 and Cu/SiO_2 did not show substantial differences, neither the choice of the active metal copper nor the selection of titania as support material alone could explain this difference in catalytic behavior. Specific metal support interactions or the particle perimeter could play an important role here. Since the activity towards the target product FA was very low, no effort was made in this study to further characterize the performance of this system. The zirconia supported copper catalyst showed a very similar behavior compared to the respective silver catalyst, but exhibited higher conversions and CO_2 selectivity. Here also, activity of zirconia resulted in methanol oxidation to CO and H_2. The selectivity towards FA is in the same low range as for Ag/ZrO_2 and thus, zirconia-based catalysts were not considered in any further catalytic studies here.

To classify the stability of the prepared catalysts under reaction conditions, long-term experiments were performed. All catalysts were tested for approximately 400 min TOS in a stream of 2.5% methanol and 1.0% oxygen in nitrogen with a total flow of 1 L_{STP} min^{-1} at 575 °C. Representative diagrams of conversion and selectivity *versus* TOS are given in Fig. 4 (for stability tests of all other systems see S2.4, Fig. S5 in the ESI†). All catalysts reached steady-state conversion and selectivity after an initial period. The product spectra revealed no significant differences compared to results obtained from temperature-dependent experiments. The Ag/SiO_2 catalyst (Fig. 4A) reached steady-state after 200 min with a FA selectivity of 86% and a methanol conversion of 76%. The catalyst with higher silver loadings prepared by sequential SEA (Fig. 4B) showed a very similar performance with approximately the same FA selectivity and methanol conversion. Silver supported on titania (Fig. 4C) also showed a steady performance with methanol conversions around 70% and FA selectivities of 75%. Interestingly, the oxygen conversion decreased to some extent with TOS although the methanol conversion remained constant. As indicated by slightly increasing H_2 selectivity and decreasing H_2O selectivity, this could be related to a reduction in hydrogen oxidation. For the Cu/SiO_2 catalysts, a more pronounced change of conversions and selectivities during an initial phase was observed. The Cu/SiO_2 catalyst prepared by single SEA (Fig. 4D) reached steady-state after 250 min with a FA selectivity of 76% and methanol conversion of 71%. The preparation of Cu/SiO_2 catalysts *via* sequential SEA (Fig. 4E)

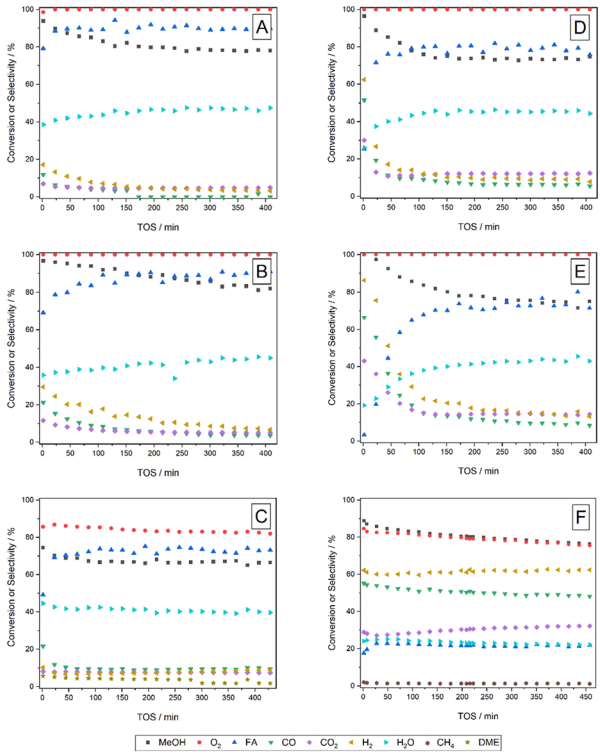

Fig. 4 Conversion and selectivity in methanol ODH as function of TOS for Ag/SiO_2 1000 m^2 L^{-1} (A), Ag/SiO_2 3 × 500 m^2 L^{-1} (B), Ag/TiO_2 1000 m^2 L^{-1} (C), Cu/SiO_2 1000 m^2 L^{-1} (D), Cu/SiO_2 3 × 500 m^2 L^{-1} (E), Cu/TiO_2 1000 m^2 L^{-1} (F). Feed: 2.5% methanol and 1.0% oxygen in nitrogen, total flow rate: 1 L_{STP} min^{-1}, reaction temperature: 575 °C.

prolonged the initial phase to 300 min but with similar catalytic properties. Copper supported on titania (Fig. 4F) reached steady operation but with a reduced selectivity to FA as compared to the silica supported systems. Formation of CO and CO_2 was favored. The activity was slightly higher than that of the pure support material.

All catalysts exhibited a stable catalytic behavior after seven hours TOS with the highest methanol conversion and FA selectivity observed for the silica-supported catalysts. Therefore, Ag/SiO_2 and Cu/SiO_2 catalysts were chosen for further comparison of silver and copper species in methanol ODH to formaldehyde and their behavior was investigated in more detail at industrially more relevant feed conditions. In this context, Ag/SiO_2 and Cu/SiO_2 systems with different metal loadings were tested at different methanol feed concentrations. The feed was varied between 2.2 and 13.1% of methanol, with a ratio of methanol to oxygen close to 2.4 and a total flow rate of 1 L_{STP} min^{-1} at a reaction temperature of 575 °C. The results determined for the Ag/SiO_2 catalysts (Fig. 5, left diagram) indicated complete oxygen conversion except for low silver loadings. There is a considerable increase in average methanol conversion with increasing silver loading (74.3% at 0.58 wt% Ag, 78.7% at 1.53 wt% Ag, 80.7% at 3.43 wt% Ag and 81.6% at 3.86 wt% Ag). Higher silver loadings appeared to increase methanol conversion although oxygen conversion is already complete. It is widely accepted that the decomposition of

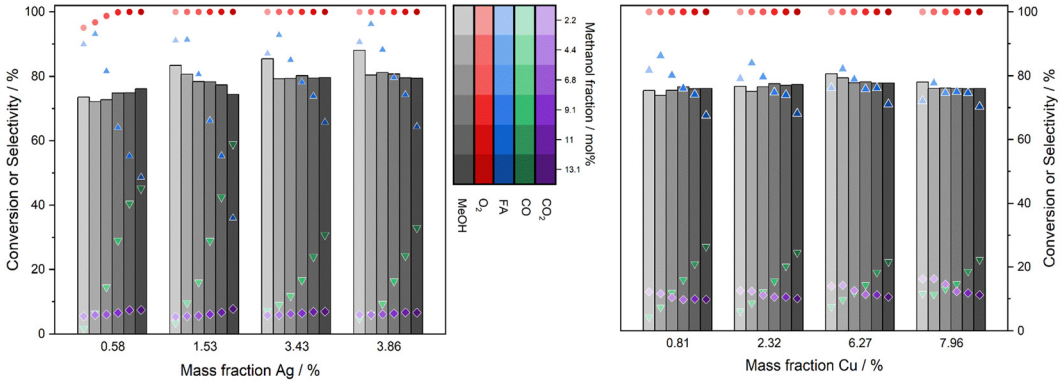

Fig. 5 Conversion and selectivity as a function of the active metal loading of the catalyst (see Table 1) and the methanol fraction in the feed (Ag/SiO_2 catalysts (left) and Cu/SiO_2 catalysts (right); reaction conditions: methanol-to-oxygen ratio 2.4, total flow rate 1 L_{STP} min^{-1}, reaction temperature 575 °C, TOS 8 h). For each metal loading, the methanol feed increases from left to right from 2.2 to 13.1% (as indicated by a change in color from light to dark grey) and is related to methanol conversion. The selectivity of the main carbon-containing products are indicated for FA (blue triangles), CO (green triangles) and CO_2 (violet diamond).

methoxy species without oxygen leads to formaldehyde by abstraction of a hydrogen atom.[12–16,18,19] This step takes place in parallel to the reaction of methoxy with oxygen to FA and OH species. In general, the presence of different oxygen species typically denoted O_α, O_β and O_γ have been reported[13,14,20,25,27,36] where O_α and O_β are surface and bulk oxygen species, respectively. O_γ forms *via* re-diffusion of O_β onto specific surface sites. Both O_α and O_γ react in the initial step of methoxy formation under abstraction of OH species, but only O_α tends to play a role in further oxidation steps like FA or CO_2 formation.[16,17,19,20] Therefore, an increase of the relative amount of O_γ compared to O_α, could increase the probability of methoxy species decomposition. This would lead directly to an increase in methanol conversion since the additional O_γ could still react with methanol. As a side effect, the selectivity towards H_2 should increase due to increased recombination of hydrogen atoms. Indeed, the observed increase in methanol conversion was accompanied by an increase in H_2 selectivity, while the selectivity to H_2O decreased accordingly (Fig. S8 in the ESI†). Since the CO selectivity did not reveal a comparable trend, FA decomposition was not the origin of the additional H_2 formation. Therefore, hydrogen was formed in the catalytic reaction. For the Ag/SiO_2 catalysts, the metal loading clearly influenced the catalytic reaction, both in terms of methanol conversion and H_2 selectivity. This is also shown for a series of catalytic tests for Ag/SiO_2 catalysts with a silver loading of 0.58, 1.15, 1.53, 3.43 and 3.86 wt% for 2.2 mol%, 2.6 mol% and 3.7 mol% methanol in the feed in Fig. S9 in the ESI,† demonstrating the reproducibility of the observed trends in methanol conversion and hydrogen selectivity over silver loading of the catalyst. As discussed, a change in relative proportion of the two relevant oxygen species considered responsible for methanol conversion could explain the experimentally observed trends. Formation of O_β depends on the oxygen solubility in bulk silver and thus on the size of the silver particles. Based on TEM analysis, the particle sizes increase with the silver loading from 1.53 wt% Ag to 3.43 wt% Ag in the Ag/SiO_2 catalysts (see ESI,† S2.3, Fig. S4). In general, an increase in particle size would be expected for increasing silver loading of the catalysts, however, this will be a subject of future investigations. Above 4.4% methanol in the feed stream (see Fig. 5), the FA selectivity decreased for all weight loadings of silver, while CO formation increased correspondingly. Higher methanol loadings generally lead to increased temperatures close to the catalyst surface since more methanol was converted in absolute numbers. Increased local temperatures were probably the cause for a more pronounced CO formation. Interestingly, the decrease in FA selectivity was lower for higher silver loadings, probably related to lower surface temperatures as indicated also by lower CO selectivities.

For the Cu/SiO_2 catalysts (Fig. 5, right diagram), the oxygen conversion was complete in all cases and the methanol conversion remained constant up to methanol feed concentrations of 13.1%. As for the silver catalyst, the selectivity to FA decreased above 4.4% methanol in the feed stream and CO selectivity increased. It is remarkable that the decline in FA selectivity was by far not as large as for the corresponding silver catalysts over the whole range of metal weight loading. For the copper catalyst, the difference in FA selectivity at low and high methanol loadings was reduced with increasing copper loading. For the catalyst with 7.96 wt% Cu the FA selectivity was nearly constant around 75% for varying methanol concentration. Comparing the silver and copper catalysts for varying methanol feed concentrations, no significant difference in average methanol conversion was found (Ag/SiO_2: 78.8% and Cu/SiO_2: 76.8%). Consistent with the previous results (Fig. 4), the silver catalysts exhibited a higher FA selectivity as the copper catalysts for low methanol feeds. With increasing methanol loading, the FA selectivity dropped significantly for Ag/SiO_2, while this decrease was less pronounced for Cu/SiO_2 resulting in a higher FA selectivity (*e.g.* at 13.1% methanol feed concentration). Additionally, the reduction in selectivity became smaller with increasing copper loading leading to nearly constant FA selectivities for 7.96 wt% Cu at all applied methanol concentrations.

Overall, this behavior illustrates that silica-supported silver catalysts exhibit higher activity towards the target product at low methanol feed concentrations but the performance of copper-based catalysts can be favorable for larger methanol fractions. In this context, the catalyst performance may be further improved by silica support materials with smaller specific surface areas. As already discussed, decomposition of FA to CO is strongly dependent on temperature and residence time. Smaller surface areas reduce the residence time within the interparticle pores of the support material and thus limit the thermal decomposition. In this manner, FA selectivities comparable to reported industrial values could also be reached for higher methanol feed concentrations.

Characterization of catalysts after reaction

The catalysts were also characterized by electron microscopy and XRD after the catalytic experiments. Representative STEM-HAADF images of the catalysts after reaction (6 h TOS) are shown in Fig. 6 for Ag/SiO_2 (A) and Cu/SiO_2 (B) (for additional TEM images and particle size distributions see S2.3, Fig. S3 and S4 in the ESI†). The silica-supported Ag particles after the catalytic reaction were rather polydisperse and in the range of 2 nm to 40 nm with an average size of 9.3 nm (with 49% of particles larger than 8 nm). Dynamic restructuring of polycrystalline silver surfaces has been reported at reaction conditions of methanol ODH.[17,22,23,26,75] A combination of thermal and oxygen-induced restructuring of the silver surface was suggested to occur under typical operation conditions.[27] For the Cu/SiO_2 catalyst, the size distribution of Cu-based particles was more narrow with an average size of 4 nm (with only 1% larger than 8 nm) and thus smaller than the respective silver catalyst. In general, a different sintering behavior of silver and copper catalysts under conditions of methanol ODH is expected as a consequence of the different melting points (1085 °C for copper, 962 °C for silver) and interactions with the support material.

The X-ray diffraction patterns after catalytic reaction are displayed in Fig. 7 for Ag/SiO_2 (A2), Cu/SiO_2 (A3) and Ag/TiO_2 (B2) (for XRD patterns of the Ag/ZrO_2, Cu/ZrO_2 and Cu/TiO_2 catalysts after reaction see Fig. S10 in the ESI†). The pure silica support (A1) revealed a very broad reflection at around 20° (2θ) which was characteristic for its amorphous structure. The titania support (B1) revealed the reflections of the anatase and rutile phase (ICDD PDF number: 98-002-4276 and 98-006-4987). The diffraction pattern measured for Ag/TiO_2 showed the reflections of the Ag phase at 39°, 43°, 65° and 77° (2θ) (ICDD PDF number: 98-005-3761). In addition to the silver reflections, larger intensities of the reflections at 28°, 37°, 42°, 54°, 57° and 69° (2θ) indicated a partial phase transformation to the rutile phase. Similar to Ag/TiO_2, the diffraction pattern of Ag/SiO_2 indicated additional reflections at 39°, 43°, 65° and 77° (2θ) corresponding to the silver particles. For the Cu/SiO_2 catalysts, reflections at 36°, 38° and 66° (2θ) were observed, which could be assigned to a CuO phase (ICDD PDF number: 98-008-7125). However, CuO was most likely not stable under conditions of methanol ODH and metallic Cu was formed at 575 °C (methanol-to-oxygen ratio of 2.5). The reduction of copper oxides to metallic copper under conditions of the silver process was previously shown by *in situ* X-ray diffraction for different gas-phase compositions of methanol and oxygen.[38] Metallic copper was formed above 127 °C (100% methanol), 427 °C to 527 °C (1 : 1 methanol/oxygen) and 677 °C (100% oxygen). Copper(II) oxide observed in the XRD diagrams most probably originates from contact with excess air after the actual catalytic tests. Similar to the silver–oxygen system, a dynamic equilibrium between gas-phase oxygen and oxygen species located on the Cu surface or in the bulk, is formed, and dynamic restructuring of copper surfaces was also reported under methanol oxidation conditions.[38,40] For the catalytic tests in this study, a steady-state is reached after an initial phase and no further deactivation of Ag/SiO_2 and Cu/SiO_2 catalysts took place after 400° min TOS. Therefore, even if surface restructuring may be not in a steady state, it does not influence the catalytic activity and stability. Based on XRD analysis after the catalytic

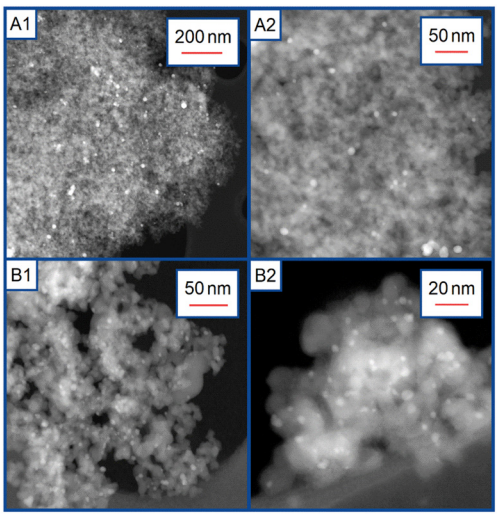

Fig. 6 STEM-HAADF images of the catalysts after catalytic reaction (A1 and A2: $AgSiO_2$ 1000 m^2 L^{-1}, B1 and B2: $CuSiO_2$ 1000 m^2 L^{-1}).

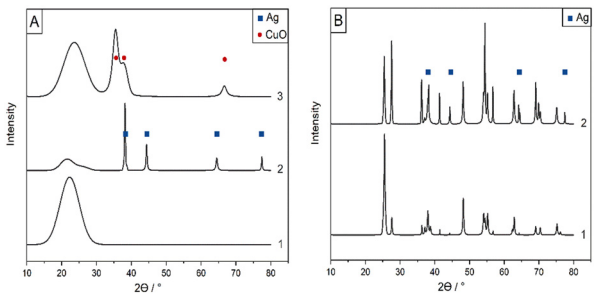

Fig. 7 XRD patterns of Ag and Cu catalysts after the catalytic reaction (after 7 h TOS at 575 °C). Silica supported catalysts (A: SiO_2 (1), Ag/SiO_2 3 × 500 m^2 L^{-1} (2), Cu/SiO_2 3 × 500 m^2 L^{-1} (3)); titania-supported catalyst (B: TiO_2 (P25) (1), Ag/TiO_2 2 × 500 m^2 L^{-1} (2)).

testing, the crystallite sizes were calculated using the Scherrer equation. The crystallite sizes of the metal particles after the catalytic tests were 36 nm for Ag/SiO_2 ($3 \times 500\ m^2\ L^{-1}$), 30 nm for Ag/TiO_2 ($2 \times 500\ m^2\ L^{-1}$) and 4 nm for Cu/SiO_2 ($3 \times 500\ m^2\ L^{-1}$) and in good agreement with the trends observed by TEM analysis. As compared to the silver catalysts, the copper catalysts revealed smaller initial adsorbate sizes and retained a small metal particle size after the catalytic tests.

Conclusion

A series of silver and copper catalysts on SiO_2, TiO_2 and ZrO_2 (*i.e.* Ag/SiO_2, Ag/TiO_2, Ag/ZrO_2, Cu/SiO_2, Cu/TiO_2 and Cu/ZrO_2) was prepared using SEA of the ammine complexes. This approach yielded small metal species homogeneously dispersed over the support materials. Thereby, adsorption of copper complexes tended to form smaller surface species compared to silver complexes and surface species tended to be smaller on titanium dioxide than on silica. By applying sequential steps of SEA, higher metal loadings up to 3.86% and 7.96% were achieved for Ag and Cu catalysts, respectively. Ag/SiO_2 and Cu/SiO_2 showed a good performance in the methanol ODH to formaldehyde with a product spectrum similar to previously reported product spectra. Ag/TiO_2 demonstrated a good selectivity towards FA with titania itself catalyzing the reaction. The Cu/TiO_2 catalyst revealed remarkable differences with only limited FA selectivity, probably influenced by metal–support interactions in this case. The zirconia-based catalysts formed selectively H_2 and CO due to the ZrO_2 activity itself but revealed no selectivity towards FA. All catalyst systems exhibited a stable activity after seven hours TOS during catalytic testing. Based on these results, Ag/SiO_2 and Cu/SiO_2 were chosen as reference catalysts for methanol ODH and their performance was tested at more industrially relevant feed conditions. For low methanol concentration in the feed, the silver catalysts exhibited higher formaldehyde yields compared to the copper catalysts. At higher methanol concentrations the Cu/SiO_2 catalyst showed a higher formaldehyde yield than the Ag/SiO_2 catalyst. Therefore, the relative performance of silver compared to copper in methanol ODH depends on the applied reaction conditions. With respect to the optimized bulk silver catalysts applied industrially, a detailed evaluation of relative performance compared to bulk copper catalysts exhibiting similar properties might lead to further insights. Both silver and copper catalysts reached constant conversion after distinct TOS suggesting that a steady-state of surface restructuring and catalytic activity was established.

Conflicts of interest

There are no conflicts to declare.

Acknowledgements

The authors would kindly thank the following colleagues, Armin Lautenbach for support with ICP-OES analysis, Michael Zimmermann for SEM/EDX imaging, Doreen Neumann-Walter for BET measurements and Sarah Essig for technical assistance. Further acknowledgement is given to the Laboratory for Electron Microscopy at KIT for STEM imaging. The authors gratefully acknowledge support by the Federal Ministry of Education and Research within the research project NAMOSYN (Grant number 03SF0566K0 and 03SF0566C1). S. B. acknowledges funding of the German Research Foundation – SFB 1441 – Project-ID 426888090 (projects B2, C2).

Notes and references

1 Merchant Research&Consulting Ltd., **https://mcgroup.co.uk/news/20140627/formaldehyde-production-exceed-52-mln-tonnes.html**, (accessed February 2021).
2 S. Kowatsch, in *Phenolic Resins: A Century of Progress*, Springer, Berlin Heidelberg, 2010.
3 J. Masamoto, K. Matsuzaki and H. Morishita, *J. Appl. Polym. Sci.*, 1993, **50**, 1307–1315.
4 P. R. McGill and T. Söhnel, *Phys. Chem. Chem. Phys.*, 2012, **14**, 858–868.
5 in *Proceedings of the International Conference on Circuits, Systems, Signals*, ed. A. J. Kralj and D. Kralj, 2000.
6 H. Liu, H. Gao, Y. Ma, Z. Gao and W. Eli, *Chem. Eng. Technol.*, 2012, **35**, 841–846.
7 J. Sun, H. Li, H. Song, Q. Wu, Y. Zhao and Q. Jiao, *RSC Adv.*, 2015, **5**, 87200–87205.
8 I. E. Wachs, *Surf. Sci.*, 2003, **544**, 1–4.
9 G. J. Millar and M. Collins, *Ind. Eng. Chem. Res.*, 2017, **56**, 9247–9265.
10 H. Sperber, *Chem. Ing. Tech.*, 1969, **41**, 962–966.
11 G. Reuss, W. Disteldorf, A. O. Gamer and A. Hilt, *Ullmann's Encyclopedia of Industrial Chemistry*, Wiley-VCH, Weinheim, 2005.
12 I. E. Wachs and R. J. Madix, *Surf. Sci.*, 1978, **76**, 531–558.
13 L. Lefferts, J. G. van Ommen and J. R. H. Ross, *Appl. Catal.*, 1986, **23**, 385–402.
14 H. Schubert, U. Tegtmeyer and R. Schlögl, *Catal. Lett.*, 1994, **28**, 383–395.
15 A. Andreasen, H. Lynggaard, C. Stegelmann and P. Stoltze, *Surf. Sci.*, 2003, **544**, 5–23.
16 G. I. N. Waterhouse, G. A. Bowmaker and J. B. Metson, *Appl. Catal., A*, 2004, **265**, 85–101.
17 G. I. N. Waterhouse, G. A. Bowmaker and J. B. Metson, *Appl. Catal., A*, 2004, **266**, 257–273.
18 J. Wang, X. Xu, J. Deng, Y. Liao and B. Hong, *Appl. Surf. Sci.*, 1997, **120**, 99–105.
19 A. C. van Veen, O. Hinrichsen and M. Muhler, *J. Catal.*, 2002, **210**, 53–66.
20 L. Lefferts, J. G. van Ommen and J. R. H. Ross, *Appl. Catal.*, 1987, **31**, 291–308.
21 D. Herein, A. Nagy, H. Schubert, G. Weinberg, E. Kitzelmann and R. Schlögl, *Z. Phys. Chem.*, 1996, **197**, 67–96.
22 G. J. Millar, M. L. Nelson and P. J. R. Uwins, *J. Catal.*, 1997, **169**, 143–156.

23 A. J. Nagy, G. Mestl, T. Rühle, G. Weinberg and R. Schlögl, *J. Catal.*, 1998, **179**, 548–559.
24 A. J. Nagy and G. Mestl, *Appl. Catal., A*, 1999, **188**, 337–353.
25 X. Bao, M. Muhler, B. Pettinger, R. Schlögl and G. Ertl, *Catal. Lett.*, 1993, **22**, 215–225.
26 X. Bao, J. V. Barth, G. Lehmpfuhl, R. Schuster, Y. Uchida, R. Schlögl and G. Ertl, *Surf. Sci.*, 1993, **284**, 14–22.
27 A. J. Nagy, G. Mestl, D. Herein, G. Weinberg, E. Kitzelmann and R. Schlögl, *J. Catal.*, 1999, **182**, 417–429.
28 G. I. N. Waterhouse, G. A. Bowmaker and J. B. Metson, *Appl. Surf. Sci.*, 2003, **214**, 36–51.
29 C. T. Campbell, *Surf. Sci.*, 1985, **157**, 43–60.
30 K. C. Prince, G. Paolucci and A. M. Bradshaow, *Surf. Sci.*, 1986, **175**, 101–122.
31 X. Bao, M. Muhler, T. Schedel-Niedrig and R. Schlögl, *Phys. Rev. B: Condens. Matter Mater. Phys.*, 1996, **54**, 2249–2262.
32 A. N. Salanov and V. I. Savchenko, *React. Kinet. Catal. Lett.*, 1997, **61**, 323–330.
33 A. I. Boronin, S. V. Koscheev and G. M. Zhidomirov, *J. Electron Spectrosc. Relat. Phenom.*, 1998, **96**, 43–51.
34 C. Wang, G. Deo and I. E. Wachs, *J. Phys. Chem. B*, 1999, **103**, 5645–5656.
35 T. C. R. Rocha, A. Oestereich, D. V. Demidov, M. Hävecker, S. Zafeiratos, G. Weinberg, V. I. Bukhtiyarov, A. Knop-Gericke and R. Schlögl, *Phys. Chem. Chem. Phys.*, 2012, **14**, 4554–4564.
36 T. E. Jones, T. C. R. Rocha, A. Knop-Gericke, C. Stampfl, R. Schlögl and S. Piccinin, *Phys. Chem. Chem. Phys.*, 2015, **17**, 9288–9312.
37 J. F. Walker, *Formaldehyde*, Reinhold Publishing Corporation, N.Y., 1st edn, 1944.
38 H. Werner, D. Herein, G. Schulz, U. Wild and R. Schlögl, *Catal. Lett.*, 1997, **49**, 109–119.
39 I. E. Wachs and R. J. Madix, *J. Catal.*, 1978, **53**, 208–227.
40 H. Bluhm, M. Hävecker, A. Knop-Gericke, E. Kleimenov, R. Schlögl, D. Teschner, V. I. Bukhtiyarov, D. F. Ogletree and M. Salmeron, *J. Phys. Chem. B*, 2004, **108**, 14340–14347.
41 M. D. Thomas, *J. Am. Chem. Soc.*, 1920, **42**, 867–882.
42 C. Mao and M. A. Vannice, *J. Catal.*, 1995, **154**, 230–244.
43 M. J. Beier, T. W. Hansen and J.-D. Grunwaldt, *J. Catal.*, 2009, **266**, 320–330.
44 E. A. Kyriakidou, O. S. Alexeev, A. P. Wong, C. Papadimitriou, M. D. Amiridis and J. R. Regalbuto, *J. Catal.*, 2016, **344**, 749–756.
45 Y. Cao, W. Dai and J. Deng, *Appl. Catal., A*, 1997, **158**, L27–L34.
46 W. Dai, Y. Cao, H. Li and J. Deng, *Chem. Lett.*, 1997, 197–198.
47 Q. Liu, Y. Cao, W. Dai and J. Deng, *Catal. Lett.*, 1998, **55**, 87–91.
48 W. Dai, J. Li, Y. Cao, Q. Liu and J. Deng, *Catal. Lett.*, 2000, **64**, 37–40.
49 W. Dai, Y. Cao, L. Ren, X. Xang, J. Xu, H. Li, H. He and K. Nan, *J. Catal.*, 2004, **228**, 80–91.
50 M. Zienkiewicz-Strzałka, S. Pasieczna-Patkowska, M. Kozak and S. Pikus, *Appl. Surf. Sci.*, 2013, **266**, 337–343.
51 C. Maldonado, J. L. G. Fierro, G. Birke, E. Martinez and P. Reyes, *J. Chil. Chem. Soc.*, 2010, **55**, 506–510.
52 Y. Aouat, G. Marom, D. Avnir, V. Gelman, G. E. Shter and G. S. Grader, *J. Phys. Chem. C*, 2013, **117**, 22325–22330.
53 V. Halperin, G. E. Shter, V. Gelman, D. M. Peselev, M. Mann-Lahav and G. S. Grader, *Catal. Sci. Technol.*, 2015, **5**, 1153–1162.
54 I. Sobczak and E. Dembowiak, *J. Mol. Catal. A: Chem.*, 2015, **409**, 137–148.
55 T. Shirman, J. Lattimer, M. Luneau, E. Shirman, C. Reece, M. Aizenberg, R. J. Madix, J. Aizenberg and C. M. Friend, *Chemistry*, 2018, **24**, 1833–1837.
56 E. D. Guerreiro, O. F. Gorriz, J. B. Rivarola and L. A. Arrua, *Appl. Catal., A*, 1997, **165**, 259–271.
57 E. D. Guerreiro, O. F. Gorriz, G. Larsen and L. A. Arrua, *Appl. Catal., A*, 2000, **204**, 33–48.
58 R. Takahashi, S. Sato, T. Sodesawa and M. Kato, *J. Sol-Gel Sci. Technol.*, 2000, **19**, 715–718.
59 T. Toupance, M. Kermarec and C. Louis, *J. Phys. Chem. B*, 2000, **104**, 965–972.
60 T. Toupance, M. Kermarec, J.-F. Lambert and C. Louis, *J. Phys. Chem. B*, 2002, **106**, 2277–2286.
61 R. S. Rao, A. B. Walters and M. A. Vannice, *J. Phys. Chem. B*, 2005, **109**, 2086–2092.
62 J. Florek-Milewska, P. Decyk and M. Ziolek, *Appl. Catal., A*, 2011, **393**, 215–224.
63 L. Jiao and J. R. Regalbuto, *J. Catal.*, 2008, **260**, 329–341.
64 J. Park and J. R. Regalbuto, *J. Colloid Interface Sci.*, 1995, **175**, 239–252.
65 M. Zeng, *Bull. Korean Chem. Soc.*, 2013, **34**, 953–956.
66 N. R. C. Fernandes Machado and V. S. Santana, *Catal. Today*, 2005, **107–108**, 595–601.
67 D. A. Palmer, M. L. Machesky, P. Bénézeth, D. J. Wesolowski, L. M. Anovitz and J. C. Deshon, *J. Solution Chem.*, 2009, **38**, 907–924.
68 G. W. Smith and H. W. Jacobson, *J. Phys. Chem.*, 1956, **60**, 1008–1012.
69 M. Pavelka and J. V. Burda, *Chem. Phys.*, 2005, **312**, 193–204.
70 T. Shoeib, R. K. Milburn, G. K. Koyanagi, V. V. Lavrov, D. K. Bohme, K. W. M. Siu and A. C. Hopkinson, *Int. J. Mass Spectrom.*, 2000, **201**, 87–100.
71 G. Ertl, H. Knözinger, F. Schüth and J. Weitkamp, *Handbook of Heterogeneous Catalysis*, Wiley-VCH, Weinheim, Germany, 2nd edn, 2008, vol. 8.
72 J. L. Bronkema and A. T. Bell, *J. Phys. Chem. C*, 2008, **112**, 6404–6412.
73 S. Sakong and A. Gros, *J. Catal.*, 2005, **231**, 420–429.
74 A. Montoya and B. S. Haynes, *J. Phys. Chem. C*, 2007, **111**, 9867–9876.
75 J. G. Serafin and S. R. Seyedmonir, *J. Mol. Catal. A: Chem.*, 1998, **131**, 157–168.